Storm-time depletions of multi-MeV radiation belt electrons observed at different pitch angles

Drozdov A.Y.[1], Aseev N.[2,3], Effenberger F.[2], Turner D. L.[4], Saikin A.[1], Shprits Y.[1,2,3]

1. Department of Earth, Planetary, and Space Sciences, University of California, Los Angeles, CA, USA
2. GFZ German Research Centre for Geosciences, Potsdam, Germany
3. Institute of Physics and Astronomy, University of Potsdam, Potsdam, Germany
4. Space Sciences Department, The Aerospace Corporation, El Segundo, CA, USA

Key points

- Almost half (up to 49%) of the studied storms result in a depletion of multi-MeV electrons, and majority of depletions (L* < 5.2) are produced by EMIC waves
- The probability of observed storm depletions of multi-MeV electrons depends on the pitch angle
- The number of storm depletions at small pitch angles is higher (increase up to 19%) than the number of depletions at high pitch angles

Abstract

During geomagnetic storms, the rapid depletion of the high-energy (several MeV) outer radiation belt electrons is the result of loss to the interplanetary medium through the magnetopause, outward radial diffusion and loss to the atmosphere due to wave-particle interactions. We have performed a statistical study of 110 storms using pitch angle resolved electron flux measurement from the Van Allen Probes mission and found that inside of the radiation belt (L*=3 - 5) the number of storms that result in depletion electrons with equatorial pitch angle $\alpha_{eq} = 30°$ is higher than number of storms that result in depletion of electrons with equatorial pitch angle $\alpha_{eq} = 75°$. We conclude that this is an indication of electron scattering by electromagnetic ion cyclotron waves. At the outer edge of the radiation belt (L* ≥ 5.2) the number of storms that result in depletion is also large (~40-50%), emphasizing the significance of the magnetopause shadowing effect and outward radial transport.

Plain Language Summary

Protons and electrons form a radiation environment around Earth that can change drastically during so called *geomagnetic storms*. In this study, we looked at 110 storms to understand how high-energy electrons can disappear due to different phenomena. We found that it is very common to observe a loss of high-energy electrons after storms. More often such a loss happens far away from the Earth as the electrons cross the boundary of the magnetosphere. However, closer to Earth the electrons are lost most likely due to the interaction with *electromagnetic ion cyclotron waves*, which play an important role in the dynamics of the radiation environment.

1. Introduction

Earth's outer radiation belt is populated by electrons (Russell & Thorne, 1970; Van Allen & Frank, 1959), including ones with energies up to several MeV, which are usually referred to as *ultra-relativistic electrons*. During geomagnetic storms, the electron fluxes exhibit irregular variations over several orders of magnitude causing enhancement or depletion of the fluxes at geostationary orbit (Anderson et al. 2015; O'Brien et al., 2001; Kilpua et al. 2015; Kim et al., 2015;) and inside of the radiation belts (Fennel et al., 2012; Friedel et al. 2002; Horne et al. 2009; Kataoka and Miyoshi, 2006; Meredith et al., 2011; Yuan and Zong, 2013a; Zhao and Li, 2013; Zhao et al. 2019). Reeves et al. (2003) showed that almost half of the storms result in a depletion or no change in electron fluxes at energies of approximately 1 - 3 MeV. Turner et al. (2013) obtained similar statistics based on a phase space density (PSD) analysis.

Launched in 2012, the Van Allen Probes mission (Mauk et al., 2013) provided measurements of the radiation belt electrons in a wide energy range at low geomagnetic latitudes, allowing the detection of nearly the full trapped population (close to 90° equatorial pitch angle). Those measurements revealed that our understanding of the ultra-relativistic electron dynamics is incomplete. One of the first results of the Van Allen Probes multi-MeV electron measurements showed the formation of the unexpected long-lived storage ring (Baker et al., 2013). The formation of such a storage ring was later explained by Shprits et al. (2013) through modeling of this event including Electromagnetic Ion Cyclotron (EMIC) waves. Mann et al. (2016) argued that EMIC waves alone cannot explain the depletion of the electrons at high-pitch angles and they are not required to define the dominant radiation belts morphology. However, Shprits et al. (2018) performed PSD analysis (see Shprits et al. 2017) and confirmed that the observed

depletion of multi-MeV electrons is consistent with localized loss processes by EMIC waves. The long-term simulation of multi-MeV electrons also requires additional loss processes (Drozdov et al. 2015) and can be successful if EMIC waves are considered (Drozdov et al. 2017). Although, the formation of the storage ring during storm time is a relatively common phenomena (Yuan and Zong, 2013b; Pinto et al. 2019), it is an example of an incomplete understanding of the multi-MeV electron dynamics.

Turner et al. (2015) performed a statistical study of 52 storm time periods (from September 2012 until February 2015), analyzing the response of the outer radiation belt electrons over a broad range of energies using the MagEIS (Blake et al., 2013) instrument on board of the Van Allen Probes. The authors showed that around 36% of the storms result in a depletion of the core electron fluxes ($\geq$ ~1 MeV) at high L-shells ($L \geq 4$). The storms were selected using the SYM-H index threshold of -50 nT, excluding consecutive (within 2 days window) events. The authors used omnidirectional electron flux measurements binned over L-shell ($\Delta L = 0.1$) and time ($\Delta t = 6h$). To categorize the response of the radiation belt to the storms, they compared maximum pre- and poststorm flux values at each energy and L-shell. The authors defined the prestorm flux from -84 h to -12 h before the minimum of the SYM-H index, and the poststorm flux from +12 h to +84 h. The event was labeled as depletion if the maximum of the poststorm flux value was lower by a factor of 2 in comparison to the maximum of the prestorm flux value.

Recently, Moya et al. (2017) and Turner et al. (2019) performed similar studies considering electrons of higher energies (up to multi-MeV) and including more storms. Moya et al. (2017) used pitch angle averaged fluxes of the first 4 years of the Van Allen Probes mission (from

September 2012 until June 2016, covering 78 storms) and binned the measurements over L-shell ($\Delta L = 0.1$) and time ($\Delta t = 4h$). They compared the maximum flux during 48h before and after the storms, excluding the main and most of the recovery phase of the storm. Turner et al. (2019) considered a longer period (from September 2012 until September 2017) and selected 110 storms. The authors used omnidirectional fluxes and followed the same methodology as described in Turner et al. (2015). Moya et al. (2017) and Turner et al. (2019) confirmed the results of previous studies showing the distinctly high probability of MeV and multi-MeV radiation belt electron depletion (~30-40%) during storms. Turner et al. (2019) reported a feature in the statistical results, where ≥1.5 MeV electrons displayed a stronger tendency for depletion during or/and after storms compared to lower energy electrons, and suggested this might be the result of losses due to interactions with EMIC waves. However, their analysis was limited to omnidirectional electron fluxes, and did not include an investigation of the electron flux dynamics at different pitch angles. An analysis of the pitch angle distribution can help to distinguish different loss mechanisms, such as magnetopause shadowing or wave particle interactions with EMIC waves (e.g. Xiang et al., 2016; 2017).

Pitch angle distributions (PAD) carry information about the nature of the processes that drive the dynamics of the radiation belts. For example, particle flux depletion due to the magnetopause shadowing effect (Li et al., 1997) causes the decrease of the flux at pitch angles closer to 90° due to drift shell splitting. This effect forms butterfly PADs near the edge of the magnetopause (West et al., 1972, 1973). EMIC waves can cause a rapid depletion of multi-MeV electron fluxes at pitch angles closer to field-aligned directions and lead to a narrowing of PADs (e.g. Drozdov et al., 2017; Li et al. 2007; Shprits et al., 2016; Usanova et al., 2014). As EMIC waves are distinctly

efficient at scattering of high-energy electrons close to being field-aligned (e.g. Ni et al., 2015), the narrow PADs are a key signature of the wave-particle interaction of multi-MeV electrons with EMIC waves.

Other physical processes can result in various shapes of PADs, such as pancake, flat top, cigar, cap, and 90°-minimum (Zhao et al., 2018). The pancake PAD is commonly observed and it is believed to be a result of pitch angle scattering due to wave-particle interactions accompanied by a loss to the atmosphere (e.g. Lyons et al., 1972). The flat top PAD can be a characteristic of electron acceleration via interactions with chorus waves (Horne et al., 2003) or a transition between pancake and butterfly PADs. Cap, cigar, and 90°-minimum PADs are observed for tens to hundreds of keV electrons and can be the result of wave-particle interactions, stretching of the magnetic field or the drift-shell-splitting effect. Additionally, the variation of the PADs can be a result of adiabatic changes.

Although, previous studies discuss the potential effect of the EMIC waves on PAD of multi-MeV electrons (e.g. Usanova et al., 2014, Zhao et al., 2018), understanding of the role of EMIC waves in depletion of the electrons during storms remains incomplete. The EMIC waves are commonly present during geomagnetic storms (Fraser et al., 2010; Halford et al., 2010; Keika et al., 2013; Saikin et al., 2016; Wang et al., 2016), however the effect of the narrowing of PAD and depletions of multi-MeV elections flux driven by EMIC waves was only studied during specific storms or short intervals (e.g. Aseev et al., 2017; Bingley et al., 2019; Engebretson et al., 2015; Shprits et al., 2016; Usanova et al., 2014). The statistical studies of the electrons PAD mainly focused on the shape of the distribution and did not consider multi-MeV electron

depletions caused by the geomagnetic storms. In this study, we focus on the depletion of multi-MeV electron fluxes during geomagnetic storms using pitch angle resolved data and statistics of 110 storms. The paper is structured as follows: Section 2 describes the data and methodology. Section 3 discusses the results, and we summarize and present the conclusions in the final section 4.

2. Data and methodology

In this study, we use measurements of the Energetic particle, Composition, and Thermal plasma (ECT) suite (Spence et al., 2013) on board of the Van Allen Probes. The ECT suite includes the Magnetic Electron Ion Spectrometer (MagEIS) (Blake et al., 2013) and the Relativistic Electron Proton Telescope (REPT) (Baker et al., 2013) instruments. We use electron measurements in the energy range from ~30 keV to ~1.7 MeV from the MagEIS instrument and multi-MeV electron measurements from 1.8 MeV to 6.3 MeV from the REPT instrument. Both MagEIS and REPT observations are pitch angle resolved. We construct 5-minute averaged REPT and MagEIS flux data, and then we use the T04s (Tsyganenko & Sitnov, 2005) magnetic field model to calculate the equatorial value of the pitch angle and generalized L-values or L* (Roederer, 1970) at every data point (with 5 minutes interval). The use of a realistic magnetic field model allows us to minimize the effects related to adiabatic variations.

We follow the methodology described by Turner et al (2015, 2019) and use the same set of 110 geomagnetic storms between September 2012 and September 2017 as in Turner et al (2019) to perform the statistical analysis. The storms are identified by the minimum of the SYM-H index during the main phase (SYM-H $\leq$ -50 nT). Storms that result in several SYM-H index minima

(e.g. so-called "double-dip" storms) within a 12-hour window are counted as one storm in the dataset. We adjust the epoch time to the lowest value of SYM-H.

To explore the electron dynamics statistically, we bin the electron flux in time ($\Delta t = 6$ hours) and L* ($\Delta L^* = 0.1$, $L^* \in [2.5; 6.0]$) for each storm. Since the equatorial pitch angle (α_{eq}) values of MagEIS and REPT measurements are different and depend on time, we linearly interpolate the electron flux onto a pitch angle grid $\alpha_{eq} \in [5^\circ; 85^\circ]$ with step size $\Delta\alpha_{eq} = 1^\circ$ before the binning. We use equatorial pitch angles to minimize the effects of adiabatic variations that can affect the pitch angle distribution. This is also a key difference in comparison with previous similar studies as described in the introduction. Also, in this study, we use T04s magnetic field model to calculate L* (previous studies used L-shell, which is calculated based on the averaged dipole field approximation around the shell).

For every energy, equatorial pitch angle, and L*, we identify the pre- and poststorm maximum flux values within 24 hours. We exclude the ±12 hours around the *storm time* (minimum SYM-H index) to avoid the strong variability of the electron flux during the main phase of the storm. Hence, the prestorm period is defined as -36 to -12 hours before the storm, and the poststorm period as +12 to +36 hours after the storm. We choose a smaller time window in comparison with previous studies to investigate rapid changes. To validate the sensitivity of the results of this study to the chosen time window, we repeat the analysis using longer time windows (72 hours) and present the results in the supplementary materials (see details below). An event is labeled as a *depletion event* if the decrease of the poststorm maximum flux value in comparison to the prestorm maximum flux value reaches a factor of 2.

To perform our statistical analysis of the electron radiation belt response, we calculate the percentage of storms that result in electron flux depletion (P_d) due to geomagnetic activity. The percentage P_d is the ratio of the number of storms that result in depletion at the specific energy, equatorial pitch angle and L* to the total number of storms.

3. Results and discussion

Since the orbit of the Van Allen Probes is not perfectly aligned with the equatorial magnetic plane, the measured 90° local pitch angle electrons correspond to lower equatorial pitch angles. Also, the maximum L* that the satellites can reach depends on the geomagnetic activity. To ensure that we have enough data points in our statistics we verify the number of valid storms (see Supplementary note S1). The storm is valid, if we can determine pre- and poststorm maximum flux values for the specific energy, equatorial pitch angle and L*. Based on the data validation, we choose our limiting parameters as maximum $\alpha_{eq} = 75^{\circ}$and $L^{*} = 5.5$, and minimum $\alpha_{eq} = 30^{\circ}$for the further analysis (see Supplementary figure S1).

Figure 1 shows the calculated percentage P_d for a 75° equatorial pitch angle. This figure is presented in the same format as Figure 2 from Turner et al. (2019) for comparison. Both figures show a similar likelihood of depletion events, even though in this study we use pitch angle resolved fluxes in comparison with omnidirectional electron fluxes used in the previous studies. The core population of electrons (close to 90° equatorial pitch angle) provides the dominant contribution to the omnidirectional flux. This explains the similarity between the two figures. Overall, Figure 1 shows that 30-40% of the storms result in a depletion of multi-MeV electrons

at $\alpha_{eq} = 75^{\circ}$ in the heart of the outer radiation belt (L* ~ 3.5 – 4.5), which indicates that previous studies reported the depletion of near-equatorial electrons. The large number of depletion events is observed down to L*=3.5, which is close to the inner edge of the outer electron radiation belts. This effect can be the result of wave-particle interactions with EMIC waves. Since the scattering of high-energy electrons by EMIC waves results in a narrowing of the pitch angle distribution, we determine the percentage of storms that result in a depletion at different pitch angles $P_d(\alpha_{eq})$ focusing on multi-MeV energies.

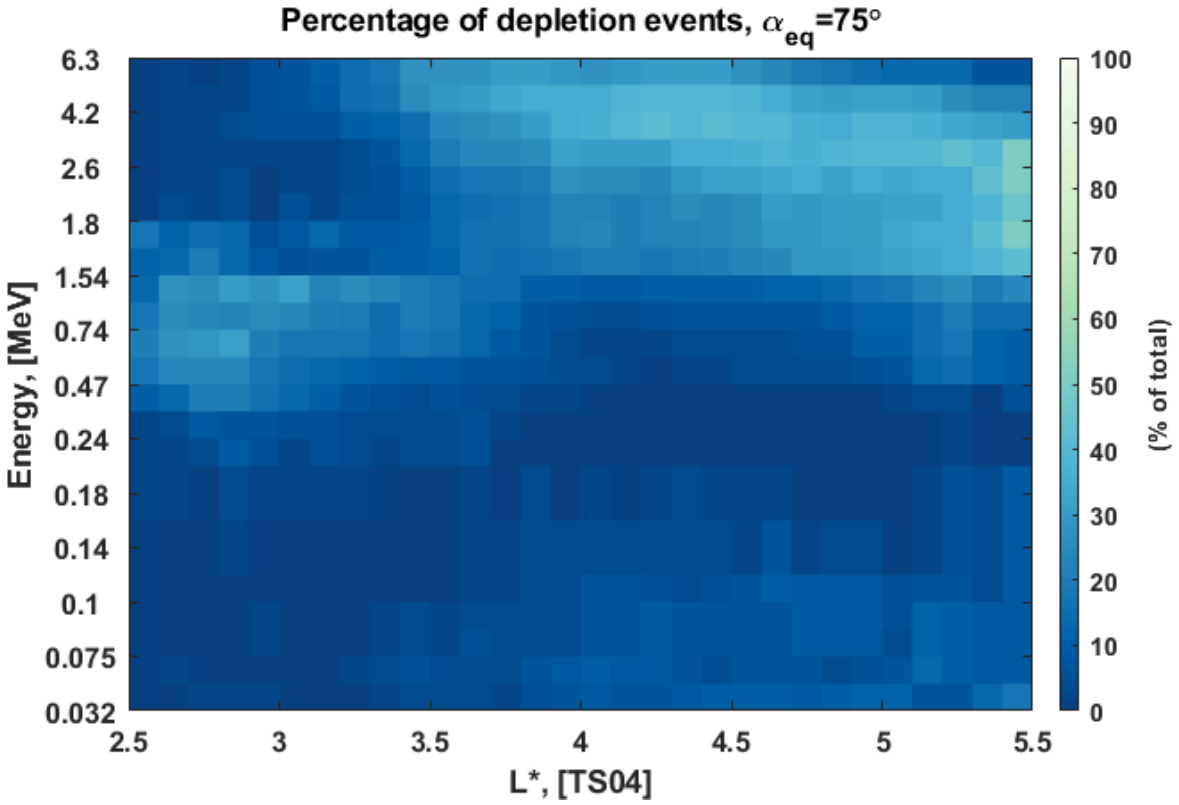

Figure 1. Percentage of events resulting in a depletion of electron fluxes as a function of L* and electron energy at a 75° equatorial pitch angle.

Figure 2 (top row) shows the percentage of depletion events for multi-MeV electrons (≥ 1.54 MeV) at different equatorial pitch angles. Also, the colorbar of the figure is chosen to enhance the differences between panels. One can see that the percentage P_d of depletion generally increases with decreasing pitch angle. The number of storms that result in the depletion of small pitch angle electrons (e.g. $\alpha_{eq} \sim 30°$) is larger than the same number of more trapped (e.g. $\alpha_{eq} \sim 75°$) electrons. Considering that such a depletion is observed at ultra-relativistic energies on a short timescale (24-hour time window), this indicates a possible scattering by EMIC waves. For a quantitative comparison, Figure 2 (bottom) shows the difference (ΔP_d) of the percentages in comparison to those at $\alpha_{eq} = 75°$, i.e.:

$$\Delta P_d(\alpha_{eq}) = P_d(\alpha_{eq}) - P_d(\alpha_{eq} = 75°).$$

The positive difference $\Delta P_d(\alpha_{eq} = 30°)$ at L* between 3 and 5 (see Figure 2e) again indicates the potential effects of EMIC waves. Also, the difference around L* 3 - 4 at energies 2.6 - 5.2 MeV is noticeably larger (up to 19%). This indicates that the electron depletion inside the outer radiation belt far from the magnetopause boundary in the energy range of effective EMIC waves scattering occurs during up to 49% of the storms.

At high L* ($L^* \geq 5.2$) the percentage P_d between 1.54 MeV and 5.2 MeV is visibly larger (~40-50%) in comparison to lower L*. This effect can be explained by magnetopause shadowing, which operates at high L*. The low percentage at higher energies (above 5.2 MeV) in the same L* region can be explained by the generally low flux level of such high-energy electrons at the outer edge of the radiation belt. The flux level can stay within the background noise indicating no change (the flux level stays within the factor of 2).

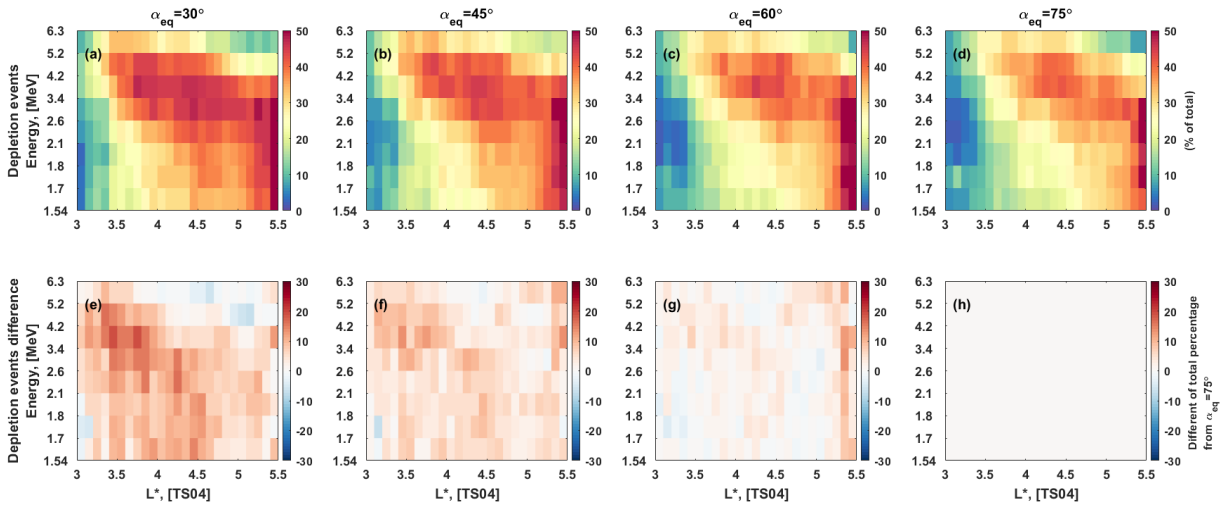

232

233 **Figure 2.** Percentage of events resulting in a depletion of multi-MeV electron fluxes as a
234 function of L* and electron energy at different equatorial pitch angle (a-d)
235 $\alpha_{eq} = 30°, 45°, 60, 75°$, respectively. (e-h) The difference of the percentages on panels (a-d) in
236 comparison to panel (d).

237

238 We perform several tests to validate our results. We repeat the analysis above for a longer pre-
239 and poststorm time window of 72 hours (see Supplementary figure S2) to ensure that the results
240 are reliable at the selected time window. We discuss the results of this analysis in Supplementary
241 note S2. Furthermore, we verify that an increase of the depletion events of multi-MeV electrons
242 with decreasing pitch angle is not a result of adiabatic changes by examining the percentage P_d
243 of the depletion events at lower energies (≤ 1.54 MeV) and different pitch angles (see Figure 3).
244 Changes in the configuration of the magnetic field can lead to the adiabatic change of the PAD.
245 For example, assuming that magnetic field line stretching is occurring, it is expected that
246 electrons of different energies will behave similarly. However, Figure 3 shows that the difference
247 ΔP_d at lower energies is negligibly small, which indicates that the positive difference ΔP_d at
248 multi-MeV energies (Figure 2) is not a result of the adiabatic changes. Finally, we investigate the

noticeably large percentage of depletion events at low L* between 2.5 and 3.5 at energies between 0.47 and 1.54 MeV (see Figure 1). We analyze the sensitivity of the result to the low flux level and conclude that the observed feature is most likely caused by errors related to the background flux level (see Supplementary note S3 and Supplementary figures S3 and S4).

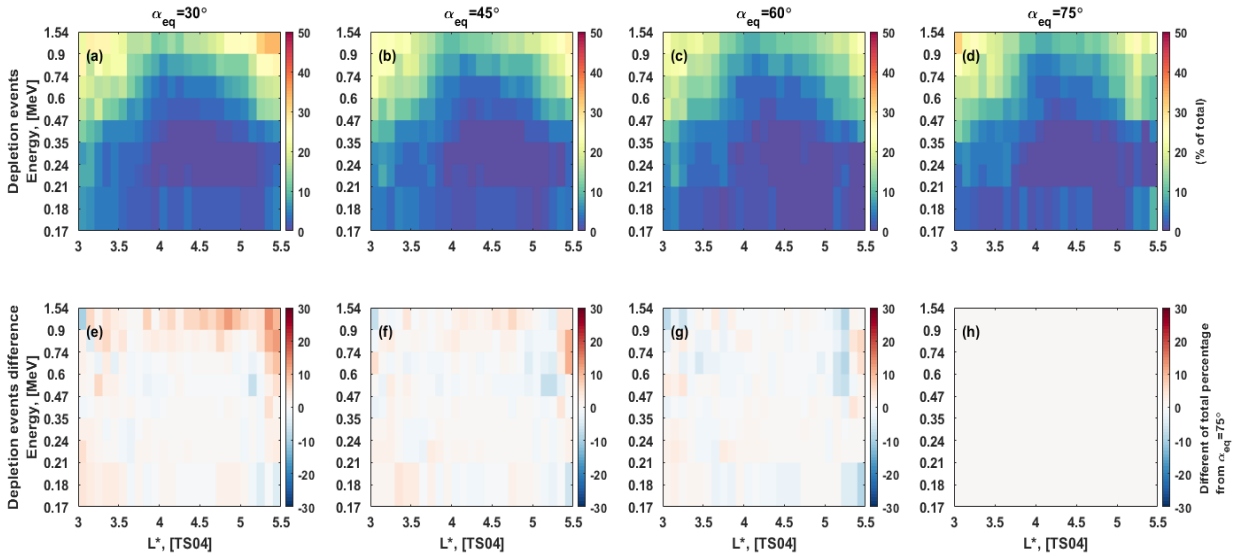

Figure 3. Same as Figure 2, but for energies between 0.17 MeV and 1.54 MeV.

To analyze the PADs we create two individual lists of the depletion events that occur at high energies of 3.4 and 4.2 MeV at $L^* = 4$ (one list per energy). For each list, we calculate prestorm PADs at 36 hours before, at 36 hours after, and poststorm PADs at 72 hours after the storm time and normalize them at $\alpha_{eq} = 75°$. From those, we analyze the depletion events with possible change of the PAD due to EMIC wave activities as discussed above. Figure 4 (c, d) shows the median of normalized PADs before and after the storm time that result in the depletion of the high-energy electrons at $\alpha_{eq} = 30°$.

The PADs after storms become narrower as energy increases, which is an indication of EMIC waves scattering. However, a narrowing of the PAD can occur due to the decrease of the magnetic field during the main phase of the storm leading to an adiabatic change. Due to the conservation of the first adiabatic invariant, the decrease of the magnetic field leads to the decrease of the perpendicular component of the electron's momentum and hence to a flatter PAD. However, as the drift shell expands during the main phase of the storm, the electron bounce trajectories shift to longer field lines. Due to the conservation of the second adiabatic invariant, the parallel component of the electron momentum decreases, leading to a narrowing of the PAD. If the change of the parallel component of the momentum is larger than the change of the perpendicular component, the resulting PAD becomes narrower. Such an adiabatic change should also be observed at lower energies. Note, that an exact estimation of the adiabatic changes is difficult because it depends on the steepness of the energy spectrum and radial gradients. However, the adiabatic changes are reversible, and the shape of the PAD can return to its initial state.

To analyze PADs at lower energies (0.47 and 0.74 MeV), we create a third list of depletion events that occur simultaneously at high energies of 3.4 and 4.2 MeV at $L^* = 4$. Figure 4 (a, b) shows that the normalized PADs of the low energy electrons also become narrower 36 hours after the storm time, however, the poststorm PADs return to the same shape as prestorm PADs. Hence, the effect of adiabatic narrowing of the PAD is almost negligible in comparison with the high-energy electrons (Figure 4 (c, d)). This indicates that EMIC wave scattering plays a potentially important role in the formation of a narrow PAD of high-energy electrons, which is

supported by the simultaneous lack of significant narrowing at lower energies, excluding an adiabatic variation effect acting at all energies (see also Supplementary figure S5).

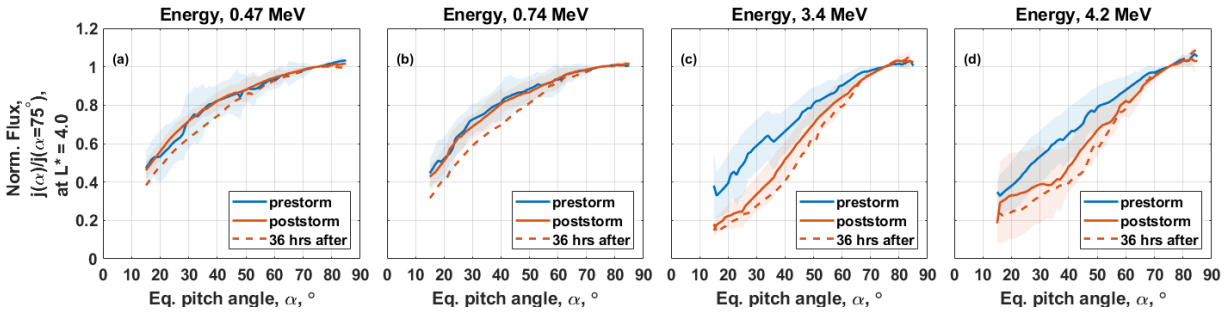

Figure 4. Normalized median PADs 36 hours before (prestorm), 36 hours after, and 72 hours after (poststorm) the storm time that result in a depletion of electrons at $\alpha_{eq} = 30^{\circ}$ at $L^{*} = 4$. (a, b) PADs of 0.47 and 0.74 MeV electrons, respectively during the depletion events at energies of 3.4 and 4.2 MeV. (c, d) PADs of 3.4 and 4.2 MeV electrons, respectively during the depletion events at the corresponding energy. The colored areas correspond to range of median absolute deviation.

4. Conclusions

In this study, we have performed a statistical analysis of 110 storms to understand the response of high-energy electrons in the outer radiation belts at different equatorial pitch angles. We found that about 30-40% of the storms result in a depletion of multi-MeV electrons (≥ 1.54 MeV) with an equatorial pitch angle of 75° in the heart of outer radiation belt (L* ~ 3.5 – 4.5). This result is in agreement with findings by Turner et al. (2019) and Moya et al. (2017) who performed a similar analysis using omnidirectional and pitch angle averaged fluxes. Analyzing the percentage of depletion events at different equatorial pitch angles, we found that more storms result in a depletion of the small pitch angle electrons ($\alpha_{eq} = 30^{\circ}$) in comparison to the near-equatorial electrons ($\alpha_{eq} = 75^{\circ}$) inside of the outer radiation belt. Specifically, the likelihood of the

depletion events exceeds 40% (reaching 49%) at L* near 3 - 4 and energies between 2.6 - 5.2 MeV and $\alpha_{eq} = 30^{\circ}$. Additionally, we investigated the rapid changes of the electron radiation belts during storms as EMIC waves can provide very fast electron scattering.

There are two possible mechanisms that can cause rapid electron depletion. The electrons can be rapidly lost due to the magnetopause shadowing effect and outward radial diffusion (Shprits et al., 2006; Turner et al., 2012). In the heart of the radiation belts (L*=4.5) and below, precipitation into the atmosphere can cause a rapid electron flux depletion due to wave-particle interactions (Green et al., 2004). Our analyses showed that a large fraction of storms result in a depletion of electrons at high L* ≥ 5.2 at all considered pitch angles, which can be explained by the magnetopause shadowing effect and outward radial diffusion. However, at lower L*, the number of storms that result in a depletion of multi-MeV electrons increases with decreasing equatorial pitch angle, which cannot be explained by outward radial diffusion or the magnetopause shadowing effect (e.g. Sibeck et al., 1987). We conclude that this effect is related to EMIC wave activity. EMIC waves can provide a rapid scattering of relativistic electrons (> 1 MeV) and are not sufficient for significant depletion of the lower energy electrons (e.g. Lyons & Thorne, 1972; Thorne & Kennel, 1971). Recent studies show that only multi-MeV electrons can be affected by EMIC waves (Drozdov et al., 2017; Mourenas et al., 2016; Pinto et al. 2019; Shprits et al., 2013, 2016, 2018; Usanova et al., 2014; Yuan et al. 2018). Our results show, that the number of depletion events of electrons below 1.54 MeV is negligible in comparison to multi-MeV electrons as the population of multi-MeV electrons requires an additional loss mechanism (e.g. Drozdov et al., 2015; Shprits et al., 2013, 2016). In addition, EMIC waves affect electrons with small pitch angles and do not resonate with the near-equatorial electrons

(e.g. Albert, 2003). As a result, more storms result in a depletion of multi-MeV electrons at $\alpha_{eq} = 30^{\circ}$ in comparison to $\alpha_{eq} = 75^{\circ}$. Also, the poststorm pitch angle distributions of the multi-MeV electrons become more narrow, representing a distinct signature of EMIC wave activity (e.g. Shprits et al., 2016; Usanova et al., 2014), while the pitch angle distributions at lower energies (< 1.54 MeV) do not show significant changes. In summary, almost half of the observed storms result in a depletion of multi-MeV electrons according to the chosen criteria. In the heart of the radiation belts, multi-MeV electron depletions show a tell-tail signature of EMIC wave activity.

5. Acknowledgments

The authors are grateful to the RBSP-ECT team for the provision of Van Allen Probes data (http://rbsp-ect.lanl.gov/). This research is supported by NASA awards 80NSSC18K0663, NNX16AF91G. The authors thank Dominika Boneberg for the help with the manuscript preparation.

6. References

Albert, J. M. (2003). Evaluation of quasi-linear diffusion coefficients for EMIC waves in a multispecies plasma. *Journal of Geophysical Research, [Space Physics]*, *108*(A6). Retrieved from https://onlinelibrary.wiley.com/doi/abs/10.1029/2002JA009792

Anderson, B. R., R. M. Millan, G. D. Reeves, and R. H. W. Friedel (2015), Acceleration and loss of relativistic electrons during small geomagnetic storms, *Geophys. Res. Lett.*, *42*(23), 10113–10119, doi:10.1002/2015GL066376.

Aseev, N. A., Y. Y. Shprits, A. Y. Drozdov, A. C. Kellerman, M. E. Usanova, D. Wang, and I. S. Zhelavskaya (2017), Signatures of Ultrarelativistic Electron Loss in the Heart of the Outer Radiation Belt Measured by Van Allen Probes, *J. Geophys. Res. [Space Phys]*, *122*(10), 2017JA024485, doi:10.1002/2017JA024485.

Baker, D. N., Kanekal, S. G., Hoxie, V. C., Batiste, S., Bolton, M., Li, X., et al. (2013). The Relativistic Electron-Proton Telescope (REPT) Instrument on Board the Radiation Belt Storm Probes (RBSP) Spacecraft: Characterization of Earth's Radiation Belt High-Energy Particle Populations. *Space Science Reviews*, *179*(1-4), 337–381. https://doi.org/10.1007/s11214-012-9950-9

Bingley, L., V. Angelopoulos, D. Sibeck, X. Zhang, and A. Halford (2019), The Evolution of a Pitch-Angle 'Bite-Out' Scattering Signature Caused by EMIC Wave Activity: A Case Study, *J. Geophys. Res. [Space Phys]*, *215*, 9, doi:10.1029/2018JA026292.

Blake, J. B., Carranza, P. A., Claudepierre, S. G., Clemmons, J. H., Crain, W. R., Jr., Dotan, Y., et al. (2013). The Magnetic Electron Ion Spectrometer (MagEIS) Instruments Aboard the Radiation Belt Storm Probes (RBSP) Spacecraft. *Space Science Reviews*, *179*(1-4), 383–421. https://doi.org/10.1007/s11214-013-9991-8

Drozdov, A. Y., Shprits, Y. Y., Orlova, K. G., Kellerman, A. C., Subbotin, D. A., Baker, D. N., et al. (2015). Energetic, relativistic, and ultrarelativistic electrons: Comparison of long-term VERB code simulations with Van Allen Probes measurements. *Journal of Geophysical Research, [Space Physics]*, *120*(5), 3574–3587. https://doi.org/10.1002/2014JA020637

Drozdov, A. Y., Shprits, Y. Y., Usanova, M. E., Aseev, N. A., Kellerman, A. C., & Zhu, H. (2017). EMIC wave parameterization in the long-term VERB code simulation. *Journal of Geophysical Research, [Space Physics]*, *122*(8), 2017JA024389.

https://doi.org/10.1002/2017JA024389

Engebretson, M. J. et al. (2015), Van Allen probes, NOAA, GOES, and ground observations of an intense EMIC wave event extending over 12 h in magnetic local time: EMIC WAVES AND THE RADIATION BELTS, *J. Geophys. Res. [Space Phys]*, *120*(7), 5465–5488, doi:10.1002/2015JA021227.

Fraser, B. J., R. S. Grew, S. K. Morley, J. C. Green, H. J. Singer, T. M. Loto'aniu, and M. F. Thomsen (2010), Storm time observations of electromagnetic ion cyclotron waves at geosynchronous orbit: GOES results: EMIC WAVES AND STORMS, GOES RESULTS, *J. Geophys. Res.*, *115*(A5), doi:10.1029/2009JA014516.

Friedel, R. H. W., G. D. Reeves, and T. Obara (2002), Relativistic electron dynamics in the inner magnetosphere — a review, *J. Atmos. Sol. Terr. Phys.*, *64*(2), 265–282, doi:10.1016/S1364-6826(01)00088-8.

Fennell, J. F., S. Kanekal, and J. L. Roeder (2012), Storm Responses of Radiation Belts During Solar Cycle 23: HEO Satellite Observations: Summers/Dynamics of the Earth's Radiation Belts and Inner Magnetosphere, in *Dynamics of the Earth's Radiation Belts and Inner Magnetosphere*, vol. 155, edited by D. Summers, I. R. Mann, D. N. Baker, and M. Schulz, pp. 371–384, American Geophysical Union, Washington, D. C.

Green, J. C., Onsager, T. G., O'Brien, T. P., & Baker, D. N. (2004). Testing loss mechanisms capable of rapidly depleting relativistic electron flux in the Earth's outer radiation belt. *Journal of Geophysical Research, 109*(A12), A12211. https://doi.org/10.1029/2004JA010579

Halford, A. J., B. J. Fraser, and S. K. Morley (2010), EMIC wave activity during geomagnetic storm and nonstorm periods: CRRES results, *J. Geophys. Res.*, *115*(A12), A12248,

394 doi:10.1029/2010JA015716.
395 Horne, R. B., M. M. Lam, and J. C. Green (2009), Energetic electron precipitation from the outer
396 radiation belt during geomagnetic storms, *Geophys. Res. Lett.*, *36*(19), 1249,
397 doi:10.1029/2009GL040236.
398 Horne, R. B., Meredith, N. P., Thorne, R. M., Heynderickx, D., Iles, R. H. A., & Anderson, R. R.
399 (2003). Evolution of energetic electron pitch angle distributions during storm time electron
400 acceleration to megaelectronvolt energies. *Journal of Geophysical Research, [Space*
401 *Physics]*, *108*(A1), SMP 11–1–SMP 11–13. https://doi.org/10.1029/2001JA009165
402 Kataoka, R., and Y. Miyoshi (2006), Flux enhancement of radiation belt electrons during
403 geomagnetic storms driven by coronal mass ejections and corotating interaction regions:
404 RADIATION BELT DURING CME/CIR STORMS, *Space Weather*, *4*(9),
405 doi:10.1029/2005SW000211.
406 Keika, K., K. Takahashi, A. Y. Ukhorskiy, and Y. Miyoshi (2013), Global characteristics of
407 electromagnetic ion cyclotron waves: Occurrence rate and its storm dependence: GLOBAL
408 CHARACTERISTICS OF EMIC WAVES, *J. Geophys. Res. [Space Phys]*, *118*(7), 4135–
409 4150, doi:10.1002/jgra.50385.
410 Kilpua, E. K. J., H. Hietala, D. L. Turner, H. E. J. Koskinen, T. I. Pulkkinen, J. V. Rodriguez, G.
411 D. Reeves, S. G. Claudepierre, and H. E. Spence (2015), Unraveling the drivers of the storm
412 time radiation belt response, *Geophys. Res. Lett.*, *42*(9), 2015GL063542,
413 doi:10.1002/2015GL063542.
414 Kim, H.-J., L. Lyons, V. Pinto, C.-P. Wang, and K.-C. Kim (2015), Revisit of relationship
415 between geosynchronous relativistic electron enhancements and magnetic storms: STORMS
416 AND ELECTRON ENHANCEMENTS AT GEO, *Geophys. Res. Lett.*, *42*(15), 6155–6161,

417 doi:10.1002/2015GL065192.
418 Li, X., Baker, D. N., Temerin, M., Cayton, T. E., Reeves, E. G. D., Christensen, R. A., et al.
419 (1997). Multisatellite observations of the outer zone electron variation during the November
420 3-4, 1993, magnetic storm. *Journal of Geophysical Research*, *102*(A7), 14123–14140.
421 https://doi.org/10.1029/97JA01101
422 Li, W., Y. Y. Shprits, and R. M. Thorne (2007), Dynamic evolution of energetic outer zone
423 electrons due to wave-particle interactions during storms, *J. Geophys. Res. [Space Phys]*,
424 112(A10), doi:10.1029/2007JA012368.
425 Lyons, L. R., & Thorne, R. M. (1972). Parasitic pitch angle diffusion of radiation belt particles
426 by ion cyclotron waves. *Journal of Geophysical Research*, *77*(28), 5608–5616.
427 https://doi.org/10.1029/JA077i028p05608
428 Lyons, L. R., Thorne, R. M., & Kennel, C. F. (1972). Pitch-angle diffusion of radiation belt
429 electrons within the plasmasphere. *Journal of Geophysical Research*, *77*(19), 3455–3474.
430 https://doi.org/10.1029/JA077i019p03455
431 Mann, I. R. et al. (2016), Explaining the dynamics of the ultra-relativistic third Van Allen
432 radiation belt, *Nat. Phys.*, doi:10.1038/nphys3799.
433 Mauk, B. H., Fox, N. J., Kanekal, S. G., Kessel, R. L., Sibeck, D. G., & Ukhorskiy, A. (2013).
434 Science Objectives and Rationale for the Radiation Belt Storm Probes Mission. *Space*
435 *Science Reviews*, *179*(1-4), 3–27. https://doi.org/10.1007/s11214-012-9908-y
436 Meredith, N. P., R. B. Horne, M. M. Lam, M. H. Denton, J. E. Borovsky, and J. C. Green (2011),
437 Energetic electron precipitation during high-speed solar wind stream driven storms, *J.*
438 *Geophys. Res.*, *116*(A5), 409, doi:10.1029/2010JA016293.
439 Mourenas, D., Artemyev, A. V., Ma, Q., Agapitov, O. V., & Li, W. (2016). Fast dropouts of

multi-MeV electrons due to combined effects of EMIC and whistler mode waves. *Geophysical Research Letters*, *43*(9), 2016GL068921. https://doi.org/10.1002/2016GL068921

Moya, P. S., Pinto, V. A., Sibeck, D. G., Kanekal, S. G., & Baker, D. N. (2017). On the Effect of Geomagnetic Storms on Relativistic Electrons in the Outer Radiation Belt: Van Allen Probes Observations: EFFECT OF STORMS ON THE RADIATION BELTS. *Journal of Geophysical Research, [Space Physics]*, *122*(11), 11,100–11,108. https://doi.org/10.1002/2017JA024735

Ni, B. et al. (2015), Resonant scattering of outer zone relativistic electrons by multiband EMIC waves and resultant electron loss time scales: ELECTRON SCATTERING BY EMIC WAVES, *J. Geophys. Res. [Space Phys]*, 120(9), 7357–7373, doi:10.1002/2015JA021466.

O'Brien, T. P., R. L. McPherron, D. Sornette, G. D. Reeves, R. Friedel, and H. J. Singer (2001), Which magnetic storms produce relativistic electrons at geosynchronous orbit?, *J. Geophys. Res.*, *106*(A8), 15533–15544, doi:10.1029/2001JA000052.

Pinto, V. A., J. Bortnik, P. S. Moya, L. R. Lyons, D. G. Sibeck, S. G. Kanekal, H. E. Spence, and D. N. Baker (2018), Characteristics, Occurrence, and Decay Rates of Remnant Belts Associated With Three-Belt Events in the Earth's Radiation Belts, *Geophys. Res. Lett.*, *45*(22), 12,099–12,107, doi:10.1029/2018GL080274.

Pinto, V. A., D. Mourenas, J. Bortnik, X. -J Zhang, A. V. Artemyev, P. S. Moya, and L. R. Lyons (2019), Decay of Ultrarelativistic Remnant Belt Electrons Through Scattering by Plasmaspheric Hiss, *J. Geophys. Res. [Space Phys]*, *119*, 2876, doi:10.1029/2019JA026509.

Reeves, G. D., McAdams, K. L., Friedel, R. H. W., & O'Brien, T. P. (2003). Acceleration and loss of relativistic electrons during geomagnetic storms. *Geophysical Research Letters*,

30(10). https://doi.org/10.1029/2002GL016513

Roederer, J. G. (1970). *Dynamics of Geomagnetically Trapped Radiation:* Springer Berlin Heidelberg. https://doi.org/10.1007/978-3-642-49300-3

Russell, C. T., & Thorne, R. M. (1970). On the Structure of the Inner Magnetosphere. In *Cosmic Electrodynamics* (Vol. 1, pp. 67–89). D. Reidel Publishing Company, Dordrecht-Holland.

Saikin, A. A., J.-C. Zhang, C. W. Smith, H. E. Spence, R. B. Torbert, and C. A. Kletzing (2016), The dependence on geomagnetic conditions and solar wind dynamic pressure of the spatial distributions of EMIC waves observed by the Van Allen Probes: RBSP EMIC WAVES, *J. Geophys. Res. [Space Phys]*, *121*(5), 4362–4377, doi:10.1002/2016JA022523.

Shprits, Y. Y., Thorne, R. M., Friedel, R., Reeves, G. D., Fennell, J., Baker, D. N., & Kanekal, S. G. (2006). Outward radial diffusion driven by losses at magnetopause. *Journal of Geophysical Research, [Space Physics]*, *111*(A11). https://doi.org/10.1029/2006JA011657

Shprits, Y. Y., Subbotin, D., Drozdov, A., Usanova, M. E., Kellerman, A., Orlova, K., et al. (2013). Unusual stable trapping of the ultrarelativistic electrons in the Van Allen radiation belts. *Nature Physics*, *9*(11), 699–703. https://doi.org/10.1038/nphys2760

Shprits, Y. Y., Drozdov, A. Y., Spasojevic, M., Kellerman, A. C., Usanova, M. E., Engebretson, M. J., et al. (2016). Wave-induced loss of ultra-relativistic electrons in the Van Allen radiation belts. *Nature Communications*, *7*, 12883. https://doi.org/10.1038/ncomms12883

Shprits, Y. Y., Horne, R. B., Kellerman, A. C., & Drozdov, A. Y. (2018). The dynamics of Van Allen belts revisited. *Nature Physics*, *14*, 102. https://doi.org/10.1038/nphys4350

Sibeck, D. G., McEntire, R. W., Lui, A. T. Y., Lopez, R. E., & Krimigis, S. M. (1987). Magnetic field drift shell splitting: Cause of unusual dayside particle pitch angle distributions during storms and substorms. *Journal of Geophysical Research*, *92*(A12), 13485.

https://doi.org/10.1029/JA092iA12p13485

Spence, H. E., Reeves, G. D., Baker, D. N., Blake, J. B., Bolton, M., Bourdarie, S., et al. (2013). Science Goals and Overview of the Radiation Belt Storm Probes (RBSP) Energetic Particle, Composition, and Thermal Plasma (ECT) Suite on NASA's Van Allen Probes Mission. *Space Science Reviews*, *179*(1), 311–336. https://doi.org/10.1007/s11214-013-0007-5

Thorne, R. M., & Kennel, C. F. (1971). Relativistic electron precipitation during magnetic storm main phase. *Journal of Geophysical Research*, *76*(19), 4446–4453. https://doi.org/10.1029/JA076i019p04446

Tsyganenko, N. A., & Sitnov, M. I. (2005). Modeling the dynamics of the inner magnetosphere during strong geomagnetic storms. *Journal of Geophysical Research*, *110*(A3), 7737. https://doi.org/10.1029/2004JA010798

Turner, D. L., Shprits, Y., Hartinger, M., & Angelopoulos, V. (2012). Explaining sudden losses of outer radiation belt electrons during geomagnetic storms. *Nature Physics*, *8*(3), 208–212. https://doi.org/10.1038/nphys2185

Turner, D. L., Angelopoulos, V., Li, W., Hartinger, M. D., Usanova, M., Mann, I. R., et al. (2013). On the storm-time evolution of relativistic electron phase space density in Earth's outer radiation belt. *Journal of Geophysical Research, [Space Physics]*, *118*(5), 2196–2212. https://doi.org/10.1002/jgra.50151

Turner, D. L., O'Brien, T. P., Fennell, J. F., Claudepierre, S. G., Blake, J. B., Kilpua, E., & Hietala, H. (2015). The effects of geomagnetic storms on electrons in Earth's radiation belts. *Geophysical Research Letters*, 2015GL064747. https://doi.org/10.1002/2015GL064747

Turner, D. L., Kilpua, E. K. J., Hietala, H., Claudepierre, S. G., O'Brien, T. P., Fennell, J. F., et al. (2019). The response of Earth's electron radiation belts to geomagnetic storms: Statistics

509 from the Van Allen Probes era including effects from different storm drivers. *Journal of*
510 *Geophysical Research, [Space Physics]*. https://doi.org/10.1029/2018JA026066
511 Usanova, M. E., Drozdov, A., Orlova, K., Mann, I. R., Shprits, Y., Robertson, M. T., et al.
512 (2014). Effect of EMIC waves on relativistic and ultrarelativistic electron populations:
513 Ground-based and Van Allen Probes observations. *Geophysical Research Letters*, *41*(5),
514 1375–1381. https://doi.org/10.1002/2013GL059024
515 Van Allen, J. A., & Frank, L. A. (1959). Radiation Around the Earth to a Radial Distance of
516 107,400 km. *Nature*, *183*(4659), 430–434. https://doi.org/10.1038/183430a0
517 Wang, D., Z. Yuan, X. Yu, S. Huang, X. Deng, M. Zhou, and H. Li (2016), Geomagnetic storms
518 and EMIC waves: Van Allen Probe observations, *J. Geophys. Res. [Space Phys]*, *121*(7),
519 6444–6457, doi:10.1002/2015JA022318.
520 West, H. I., Jr., Buck, R. M., & Walton, J. R. (1972). Shadowing of Electron Azimuthal-Drift
521 Motions near the Noon Magnetopause. *Nature Physical Science*, *240*, 6.
522 https://doi.org/10.1038/physci240006a0
523 West, H. I., Jr., Buck, R. M., & Walton, J. R. (1973). Electron pitch angle distributions
524 throughout the magnetosphere as observed on Ogo 5. *Journal of Geophysical Research*,
525 *78*(7), 1064–1081. https://doi.org/10.1029/JA078i007p01064
526 Xiang, Z. et al. (2016), Multi-satellite simultaneous observations of magnetopause and
527 atmospheric losses of radiation belt electrons during an intense solar wind dynamic pressure
528 pulse, *Ann. Geophys.*, 34(5), 493–509, doi:10.5194/angeo-34-493-2016.
529 Xiang, Z., W. Tu, X. Li, B. Ni, S. K. Morley, and D. N. Baker (2017), Understanding the
530 Mechanisms of Radiation Belt Dropouts Observed by Van Allen Probes, *J. Geophys. Res.*
531 *[Space Phys]*, 122(10), 9858–9879, doi:10.1002/2017JA024487.

Yuan, C., and Q. Zong (2013a), Relativistic electron fluxes dropout in the outer radiation belt under different solar wind conditions, *J. Geophys. Res. [Space Phys]*, *118*(12), 7545–7556, doi:10.1002/2013JA019066.

Yuan, C., and Q. Zong (2013b), The double-belt outer radiation belt during CME- and CIR-driven geomagnetic storms, *J. Geophys. Res. [Space Phys]*, *118*(10), 6291–6301, doi:10.1002/jgra.50564.

Zhao, H., and X. Li (2013), Inward shift of outer radiation belt electrons as a function of Dst index and the influence of the solar wind on electron injections into the slot region, *J. Geophys. Res. [Space Phys]*, *118*(2), 756–764, doi:10.1029/2012JA018179.

Yuan, Z., K. Liu, X. Yu, F. Yao, S. Huang, D. Wang, and Z. Ouyang (2018), Precipitation of Radiation Belt Electrons by EMIC Waves With Conjugated Observations of NOAA and Van Allen Satellites, *Geophys. Res. Lett.*, *45*(23), A07209, doi:10.1029/2018GL080481.

Zhao, H., Friedel, R. H. W., Chen, Y., Reeves, G. D., Baker, D. N., Li, X., et al. (2018). An Empirical Model of Radiation Belt Electron Pitch Angle Distributions Based On Van Allen Probes Measurements. *Journal of Geophysical Research, [Space Physics]*, *123*(5), 3493–3511. https://doi.org/10.1029/2018JA025277

Zhao, H., D. N. Baker, X. Li, A. N. Jaynes, and S. G. Kanekal (2019), The Effects of Geomagnetic Storms and Solar Wind Conditions on the Ultrarelativistic Electron Flux Enhancements, *J. Geophys. Res. [Space Phys]*, *124*(3), 1948–1965, doi:10.1029/2018JA026257.

Figure 1.

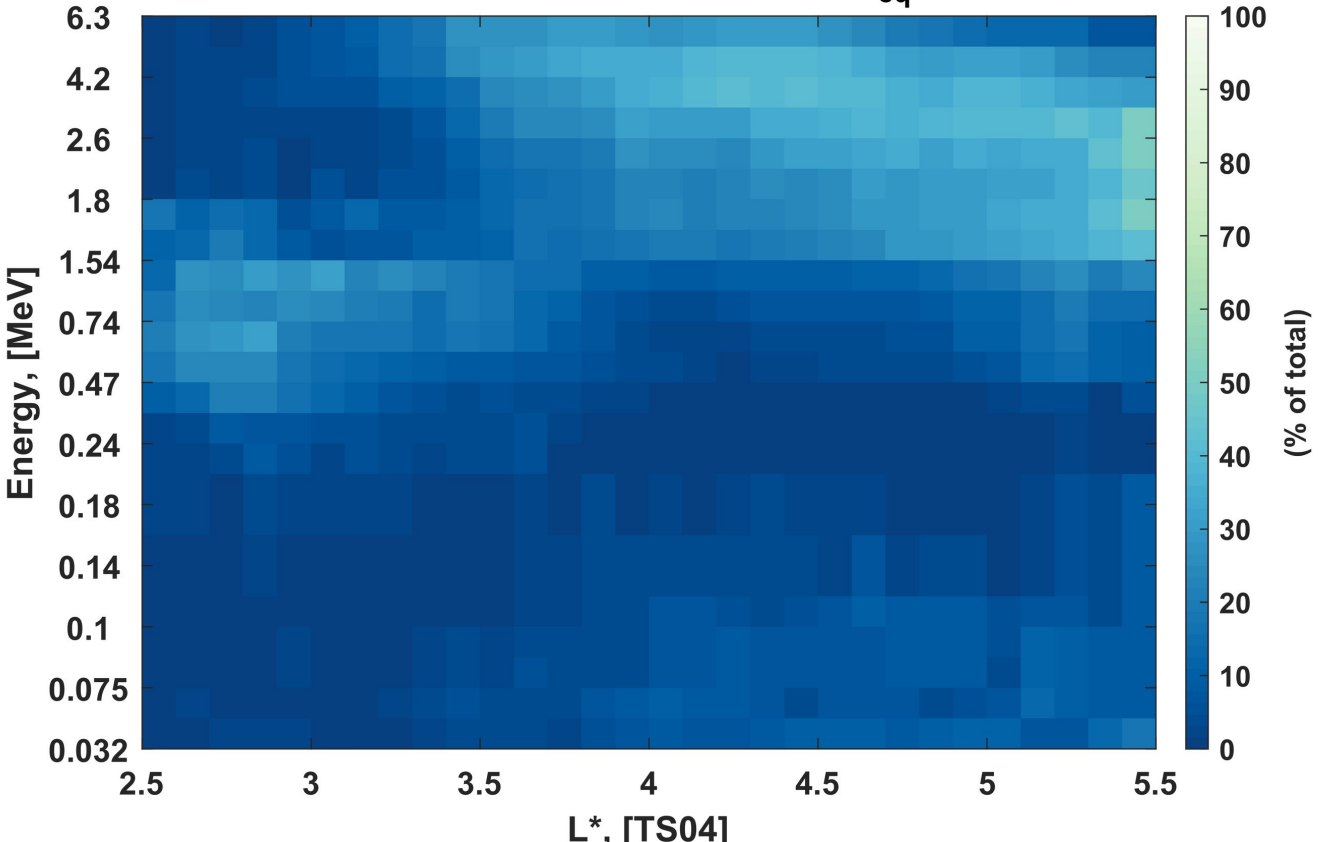
Percentage of depletion events, α_{eq}=75°
Energy, [MeV]
6.3
4.2
2.6
1.8
1.54
0.74
0.47
0.24
0.18
0.14
0.1
0.075
0.032
2.5
3
3.5
4
4.5
5
5.5
L*, [TS04]
100
90
80
70
60
50
40
30
20
10
0
(% of total)

Figure 2.

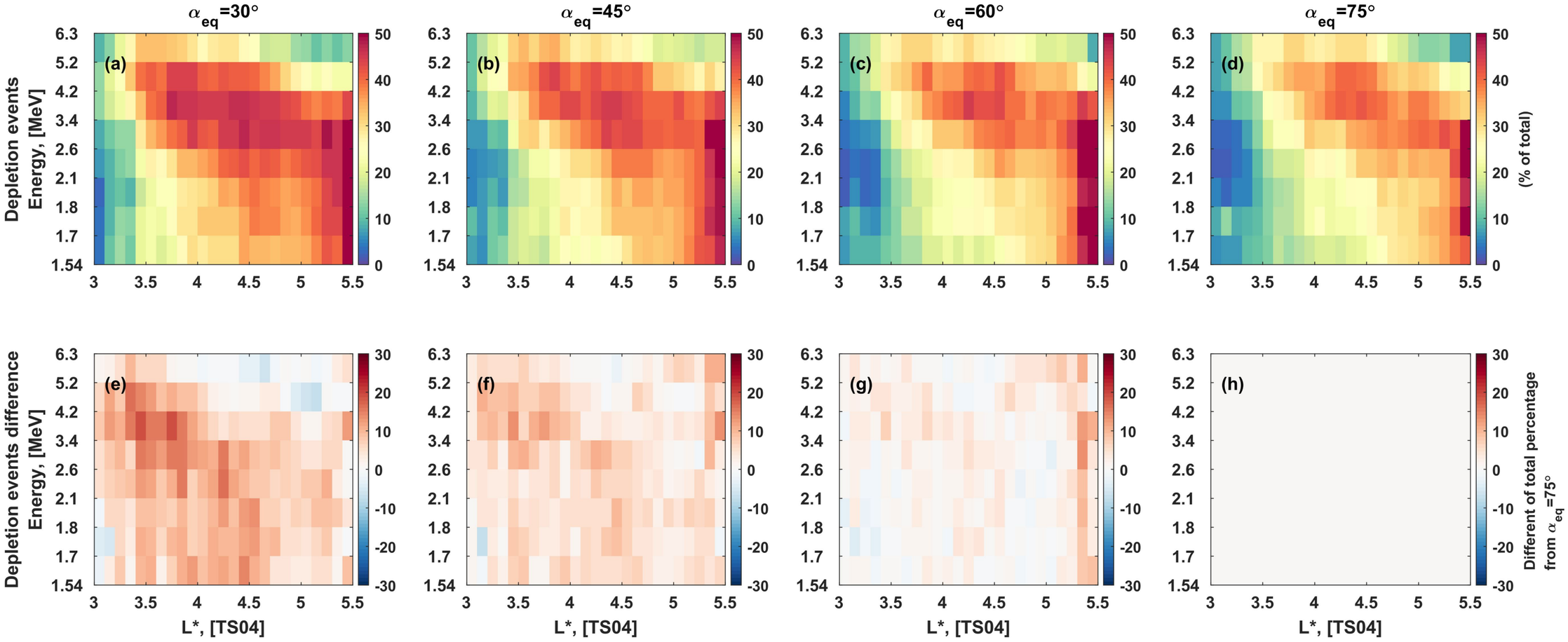
α_{eq}=30°
α_{eq}=45°
α_{eq}=60°
α_{eq}=75°
(a)
(b)
(c)
(d)
(e)
(f)
(g)
(h)
Depletion events
Energy, [MeV]
Depletion events difference
Energy, [MeV]
L*, [TS04]
(% of total)
Different of total percentage
from α_{eq}=75°
6.3
5.2
4.2
3.4
2.6
2.1
1.8
1.7
1.54
3
3.5
4
4.5
5
5.5
50
40
30
20
10
0
-10
-20
-30

Figure 3.

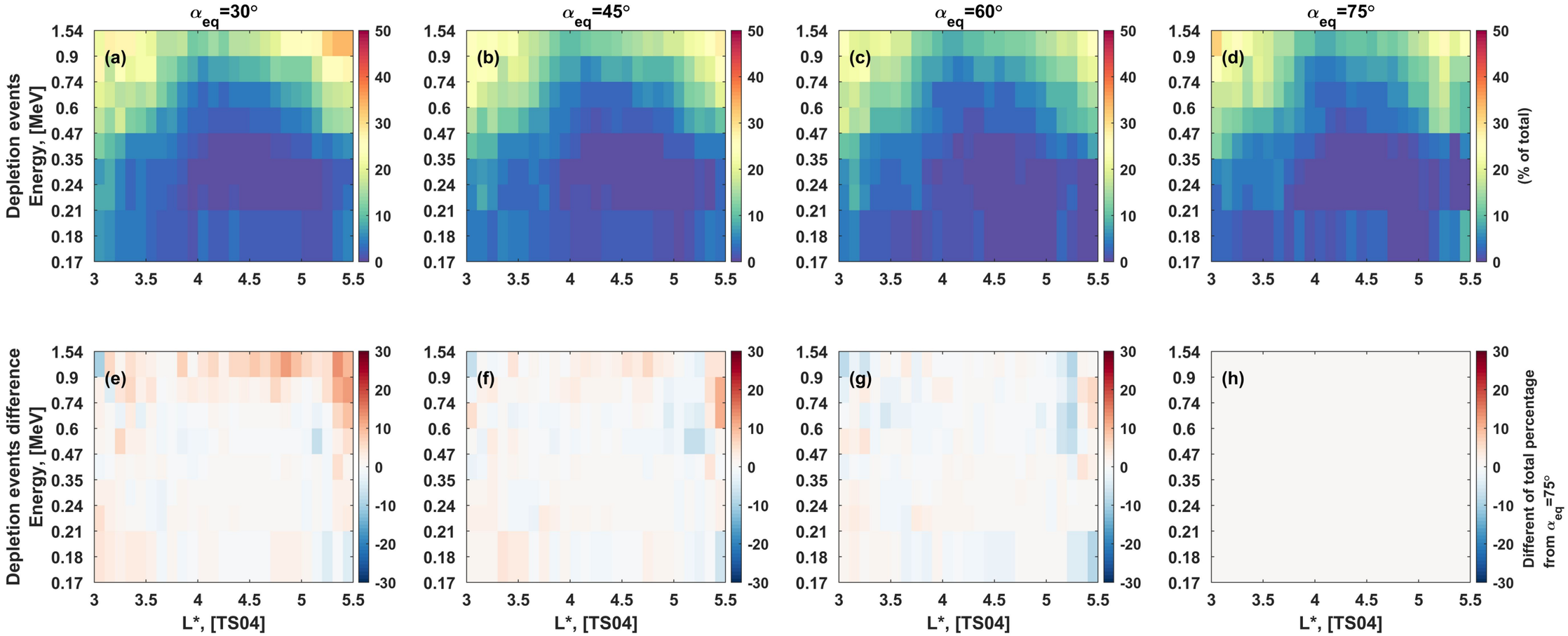
α_{eq}=30°
α_{eq}=45°
α_{eq}=60°
α_{eq}=75°
(a)
(b)
(c)
(d)
(e)
(f)
(g)
(h)
Depletion events
Energy, [MeV]
Depletion events difference
Energy, [MeV]
L*, [TS04]
(% of total)
Different of total percentage
from α_{eq}=75°
1.54
0.9
0.74
0.6
0.47
0.35
0.24
0.21
0.18
0.17
3
3.5
4
4.5
5
5.5
50
40
30
20
10
0
-10
-20
-30

Figure 4.

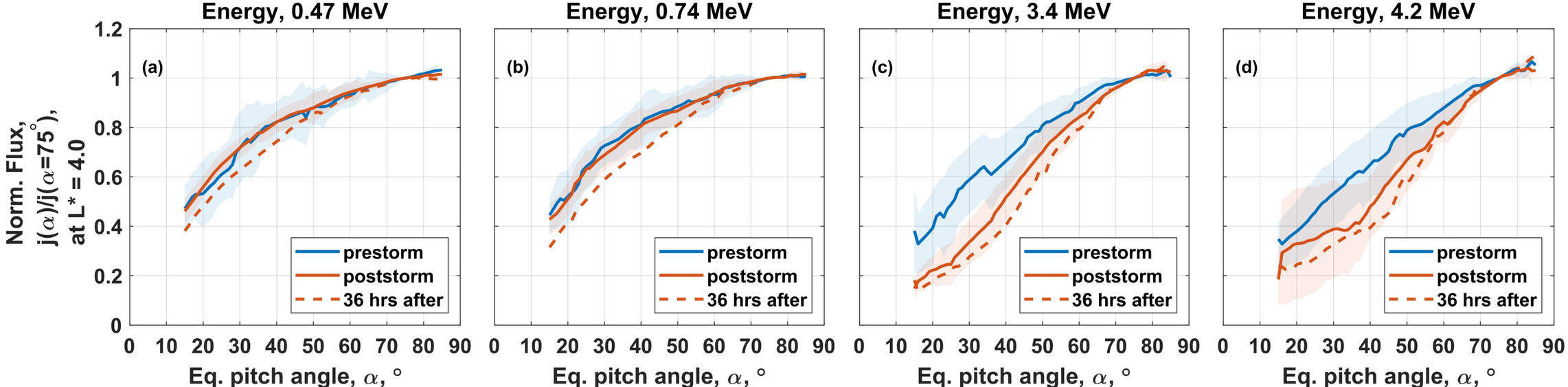
Energy, 0.47 MeV
Energy, 0.74 MeV
Energy, 3.4 MeV
Energy, 4.2 MeV
(a)
(b)
(c)
(d)
Norm. Flux,
j(α)/j(α=75°),
at L* = 4.0
prestorm
poststorm
36 hrs after
Eq. pitch angle, α, °
0
0.2
0.4
0.6
0.8
1
1.2
0 10 20 30 40 50 60 70 80 90